



HAL
open science

Dispersion properties and low infrared optical losses in epitaxial AlN on sapphire substrate in the visible and infrared range

Ali Soltani, Arnaud Stolz, Joël Charrier, Maghnia Mattalah, Jean-Claude Gerbedoen, Hassan Ali Barkad, Vincent Mortet, Michel Rousseau, Nour Eddine Bourzgui, Ali Benmoussa, et al.

► To cite this version:

Ali Soltani, Arnaud Stolz, Joël Charrier, Maghnia Mattalah, Jean-Claude Gerbedoen, et al.. Dispersion properties and low infrared optical losses in epitaxial AlN on sapphire substrate in the visible and infrared range. *Journal of Applied Physics*, 2014, 115 (16), pp.163515. 10.1063/1.4873236 . hal-00987345

HAL Id: hal-00987345

<https://hal.science/hal-00987345>

Submitted on 25 May 2022

HAL is a multi-disciplinary open access archive for the deposit and dissemination of scientific research documents, whether they are published or not. The documents may come from teaching and research institutions in France or abroad, or from public or private research centers.

L'archive ouverte pluridisciplinaire **HAL**, est destinée au dépôt et à la diffusion de documents scientifiques de niveau recherche, publiés ou non, émanant des établissements d'enseignement et de recherche français ou étrangers, des laboratoires publics ou privés.

Dispersion properties and low infrared optical losses in epitaxial AlN on sapphire substrate in the visible and infrared range

Cite as: J. Appl. Phys. **115**, 163515 (2014); <https://doi.org/10.1063/1.4873236>

Submitted: 20 November 2013 • Accepted: 14 April 2014 • Published Online: 29 April 2014

A. Soltani, A. Stolz, J. Charrier, et al.



View Online



Export Citation



CrossMark

ARTICLES YOU MAY BE INTERESTED IN

[Second harmonic generation in phase matched aluminum nitride waveguides and micro-ring resonators](#)

Applied Physics Letters **100**, 223501 (2012); <https://doi.org/10.1063/1.4722941>

[17000%/W second-harmonic conversion efficiency in single-crystalline aluminum nitride microresonators](#)

Applied Physics Letters **113**, 131102 (2018); <https://doi.org/10.1063/1.5042506>

[The temperature dependence of the refractive indices of GaN and AlN from room temperature up to 515 °C](#)

Journal of Applied Physics **104**, 106101 (2008); <https://doi.org/10.1063/1.3021148>

Lock-in Amplifiers
up to 600 MHz



Zurich
Instruments



Dispersion properties and low infrared optical losses in epitaxial AlN on sapphire substrate in the visible and infrared range

A. Soltani,^{1,a)} A. Stolz,¹ J. Charrier,² M. Mattalah,³ J.-C. Gerbedoen,¹ H. A. Barkad,⁴ V. Mortet,⁵ M. Rousseau,¹ N. Bourzgui,¹ A. BenMoussa,⁶ and J.-C. De Jaeger¹

¹*Institut d'Électronique, Microélectronique et Nanotechnologie, UMR-CNRS 8520, PRES Université Lille Nord de France, Cité Scientifique, Avenue Poincaré, CS 60069, 59652 Villeneuve d'Ascq Cedex, France*

²*Fonctions Optiques pour les Technologies de l'information, UMR-CNRS 6082, ENSSAT 6, rue de Kerampont, CS 80518, 22305 Lannion Cedex, France*

³*Laboratoire de Microélectronique, Université Djilali Liabes, 22000 Sidi Bel Abbes, Algeria*

⁴*Institut Universitaire Technologique Industriel, Université de Djibouti, Avenue Georges Clémenceau, BP 1904 Djibouti, Djibouti*

⁵*Institute of Physics of Academy of Sciences of Czech Republic, Fyzikální ústav AV CR, v.v.i., Na Slovance 1999/2, Czech Republic*

⁶*Solar Terrestrial Center of Excellence, Royal Observatory of Belgium, Circular 3, B-1180 Brussels, Belgium*

(Received 20 November 2013; accepted 14 April 2014; published online 29 April 2014)

Optical waveguiding properties of a thick wurtzite aluminum nitride highly [002]-textured hetero-epitaxial film on (001) basal plane of sapphire substrate are studied. The physical properties of the film are determined by X-ray diffraction, atomic force microscopy, microRaman, and photocurrent spectroscopy. The refractive index and the thermo-optic coefficients are determined by *m-lines* spectroscopy using the classical prism coupling technique. The optical losses of this planar waveguide are also measured in the spectral range of 450–1553 nm. The lower value of optical losses is equal to 0.7 dB/cm at 1553 nm. The optical losses due to the surface scattering are simulated showing that the contribution is the most significant at near infrared wavelength range, whereas the optical losses are due to volume scattering and material absorption in the visible range. The good physical properties and the low optical losses obtained from this planar waveguide are encouraging to achieve a wide bandgap optical guiding platform from these aluminum nitride thin films. © 2014 AIP Publishing LLC. [<http://dx.doi.org/10.1063/1.4873236>]

I. INTRODUCTION

Wurtzite-Aluminum Nitride (w-AlN) is a wide band-gap (6.2 eV) semiconductor attracting considerable attention for many applications in micro- and opto-electronics, as for photonic waveguide,¹⁶ photo-detector in X-UV range,^{1,2,18} or acoustic wave device.²⁴ Its physical properties, such as high thermal stability and high electrical behavior permit, to consider AlN as a serious candidate for high frequency, high power, and high temperature optoelectronic applications.

In order to consider a nitride-based all-optic system, optical waveguide channel have to be investigated. Present GaN-based optical waveguide on sapphire need a lattice match layer as $\text{Al}_x\text{Ga}_{1-x}\text{N}$ with low x content.⁹ In comparison, AlN-based waveguiding structure can be formed by a thin film directly grown on sapphire (Al_2O_3) substrate because it has a lower refractive index than AlN. The growth of c-oriented AlN on (001) sapphire exhibits a lattice mismatch of about 12.4%. Despite of this, a high density of threading dislocations in the order of 10^9 cm^{-2} – 10^{10} cm^{-2} exists in the AlN films, reducing the ability to consider AlN as a relevant material for waveguide optoelectronic devices where the propagation losses must be as low as possible. In the same way, refractive index values must be accurately controlled for good optical confinement if used in

semiconductor laser devices for instance. Since the optical performance is strongly influenced by the surface characteristics, good AlN quality is crucial.

In this paper, a study of an AlN waveguide structure on Al_2O_3 is presented. X-Ray Diffraction (XRD), microRaman, and photocurrent spectroscopy are performed to exhibit an adapted micro-structure to optical waveguide requirements. By using the prism coupling technique, the optical properties, such as refractive index, thermo-optic properties, and optical losses of AlN film, are measured and analyzed. The refractive index dispersion parameters as a function of the wavelength and the temperature are determined by curve fitting. Finally, planar waveguide propagation losses are evaluated as a key device parameter for telecommunication applications.

II. EXPERIMENTAL MEASUREMENT: XRD AND MICRORAMAN ANALYSIS

A single layer of undoped w-AlN on c-plane Al_2O_3 substrate (430 μm thick) is obtained from DOWA Electronics Materials Co. (Japan). The layer is grown by metal-organic chemical vapor deposition at 1100 °C under 100 mTorr pressure using high-purity ammonia and trimethylaluminum as the nitrogen (N_2) and aluminum (Al) source, respectively. The AlN epilayer shows an electron concentration below $2 \times 10^{14}\text{ cm}^{-3}$. Prior to any other processes, a substrate

^{a)}Electronic mail: ali.soltani@iemn.univ-lille1.fr

cleaning procedure has been developed based on hydrochloric and nitric acid solutions followed by acetone and isopropyl-alcohol solutions and dried under N_2 at room temperature.

XRD analysis is performed at normal and grazing incidences with a Siemens D5000 diffractometer using $CuK\alpha 1$ radiation ($\lambda = 0.1540598$ nm) operating at 40 kV and 30 mA. The rocking curve scan is performed with a detector at $2\theta = 36.15^\circ$ (Fig. 1) corresponding to the w-AlN (0002) reflection when the sample orientation θ varies from 5° to 30° .

The X-ray rocking curve at full width at half maximum is 75 arcsec (0002). The film thickness is determined by profilometer (Dektak2000) and is equal to $1 \mu\text{m}$.

MicroRaman spectra are measured using a Jobin Yvon spectrometer under an excitation wavelength at 266 nm as shown in Fig. 2. It exhibits clearly the vibrational states of AlN: $A_1(\text{TO})$ at 618 cm^{-1} , the $E_2(\text{TO})$ at 662 cm^{-1} , and the $A_1(\text{LO})$ at 891 cm^{-1} , which are close to those of a single-crystal.⁷

III. RESULTS AND DISCUSSION

A. Photocurrent spectroscopy

To investigate the photocurrent properties, 2 mm-sized circular interdigitated electrodes are patterned through optical lithography. A TiN/Au (5/150 nm) Schottky contact is deposited on the AlN surface using radio-frequency

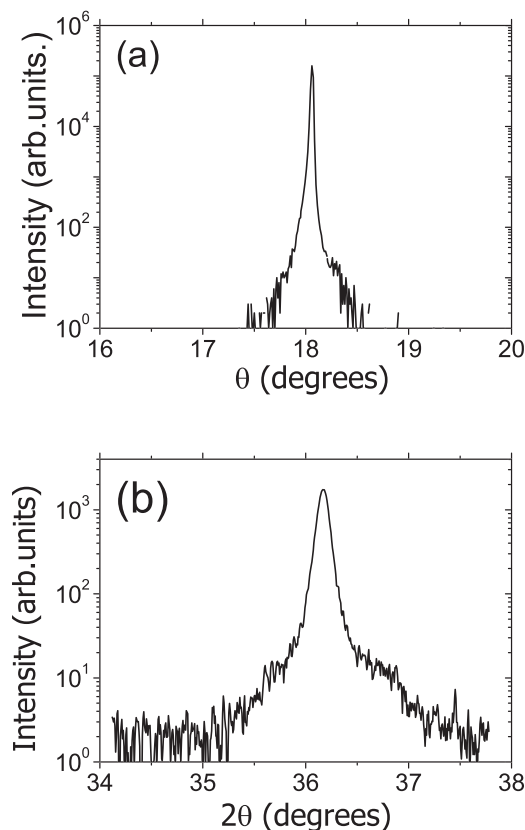


FIG. 1. XRD spectra of AlN film on Al_2O_3 substrate (a) in the θ - θ mode and (b) in the θ - 2θ rocking curve mode.

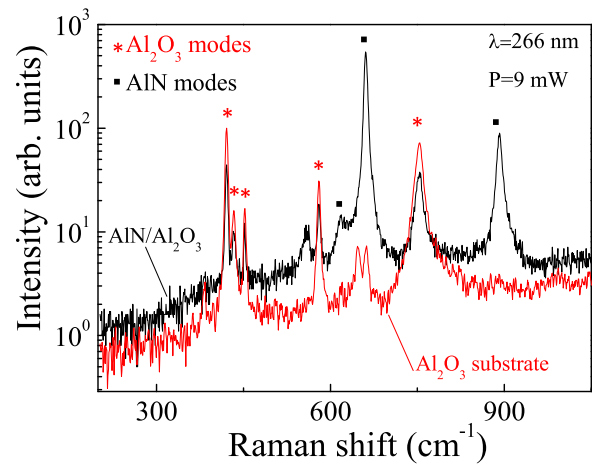


FIG. 2. MicroRaman spectra collected from w-AlN/ Al_2O_3 film. Red line is related to Al_2O_3 substrate microRaman spectrum, as the black one to AlN on Al_2O_3 . The squares are assigned to w-AlN modes and the stars are assigned to Al_2O_3 substrate modes.

magnetron sputtering. After the deposition, the electrodes are obtained by Au etching in a potassium iodide (KI) solution and by a TiN etching using a H_2SO_4/H_2O_2 solution. Sample is then annealed at 500°C for 40 min in N_2 atmosphere to improve the stability of the electrode and to form the Schottky contact.

The optical measurement in the 190–400 nm spectral range are carried out using a collimated and tunable monochromatic light beam emitted by a 30 W deuterium light source combined with a monochromator and a digital lock-in amplifier system. Absolute calibration is obtained using a silicon photodiode calibrated at the National Institute of Standards and Technology (NIST) and operating as a reference detector. The spectral resolution of the optical system is typically 1 nm.

As seen in the inset of Fig. 3, the external quantum efficiency (EQE) and the UV/visible rejection ratio have been measured. Our AlN metal-semiconductor-metal (MSM) photodetector is sensitive showing the detector band edge around 202 nm, which corresponds approximately to the energy bandgap of the AlN material. A visible rejection (between 200 and 400 nm) of more than five orders

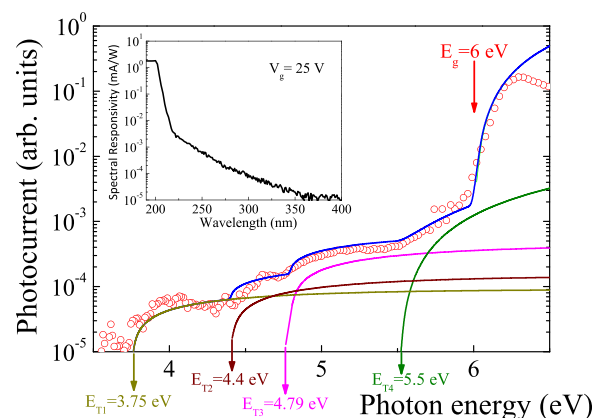


FIG. 3. Spectral photocurrent of an AlN MSM photodiode measured at $\pm 5 \text{ V}$ bias. The inset shows the spectral responsivity (mA/W) at $+25 \text{ V}$ bias between the MSM interdigitated electrodes.

magnitude is measured which is one to two orders of magnitude higher compared to AlN photodetectors that have been already reported^{1,2,6,11} probably due to a better AlN material quality and or better contact formation. No internal photoconductive gain was observed on our large AlN photodetectors (up to 4.3 mm diameter). There are stable under photon irradiation with a negligible low dark current of 3–6 pA/cm² at +15 V bias.³

Spectra of the sub-band gap absorption are usually decomposed into “band to defect” and “band to tail” type transitions. In the first case, the photocurrent I_{ph} proportionally varies with the capture cross section of traps by the relationship

$$s(h\nu) \equiv \frac{\Delta I_{ph}}{I_{dark} \phi_0 t}, \quad (1)$$

with $\Delta I_{ph} = I_{ph} - I_{dark}$. The illumination time is 62 ms and the incident photon flux per cm² is $\phi_0 = P/(S.E)$ where P is the incident power and E is the photon energy for an active area S equal to 2.2 mm². The resulting fitting parameters obtained from Inkson’s model¹⁰ are listed in Table I. Four trap levels are deduced at $E_{T1} = 3.75$ eV, $E_{T2} = 4.4$ eV, $E_{T3} = 4.79$ eV, and $E_{T4} = 5.5$ eV up to the valence band, as shown in Fig. 3.

It should be noticed that there are only few studies giving calculation characteristics of defects in the w-AlN band structure as vacancies centers or extended defects. The capture cross sections of E_{T1} , E_{T2} , and E_{T3} show that those transitions are vertically allowed and non-vertically forbidden for E_{T4} . The transition E_{T3} is responsible of the exponential increase at the absorption edge commonly described by the Urbach’s rule²⁸ and follows the relation:

$$I_{ph}(E) = I_{ph0} \exp\left(\frac{E - E_G}{E_U}\right), \quad (2)$$

where I_{ph0} is a material parameter, E_G is the band gap energy, and E_U is the Urbach energy representing the width of the exponential absorption edge. In the particular case of III-nitride materials, the Urbach’s tail is mainly a consequence of the carrier interaction with lattice and lattice imperfections (as defects or impurities). The photocurrent curve is fitted with the Urbach expression (2) giving E_G , I_{ph0} , and E_U equals to 6 eV, 4.45×10^{-4} , and 0.13 eV, respectively. The capture cross section increases when the trap level is very deep. The small ones values correspond to negatively charged center levels.⁴ According to Silvestri *et al.*,²¹ the centers vacancies (N-V, Al-V) could be a possible source of defect in our sample.^{12,14,19,20}

B. M-lines spectroscopy: Index dispersion

Optical characterization is performed using a commercial Metricon M2010 system. This setup is mainly based on the prism-coupling technique.²⁶ Light penetrates through a TiO₂ prism ($A_p = 60^\circ$) into the sample by evanescent wave. Effective guided modes are highlighted from reflectivity drops out of the prism. From values of specific incident angle α_m for transverse electric (TE) or transverse magnetic (TM) polarization, at each wavelength, the corresponding effective-mode index N_m is computed as described in Ref. 22. The relative error of this system is 10^{-3} . Refractive index (n) in TE/TM polarization is then available by injecting the N_m values into a propagation law based on Maxwell’s equations.²⁷

Laser sources (with highest power below 4 mW·cm⁻²) are used to cover the spectral range from 450 nm to 1553 nm. Fig. 4 presents a dispersion curve with a comparison with single crystal values, computed from a Sellmeier calculation with experimental coefficients¹⁵ using the following equation:

$$n^2 = C_1 + \frac{C_2 \lambda^2}{\lambda^2 - C_3} + \frac{C_4 \lambda^2}{\lambda^2 - C_5}. \quad (3)$$

From our measurement, extracted fitting coefficient values are: $C_1 = 2.66$, $C_2 = 1.5$, $C_3 = 0.185$, $C_4 = 8$, $C_5 = 20$ and $C_1 = 2.64$, $C_2 = 1.7$, $C_3 = 0.185$, $C_4 = 3$, $C_5 = 20$ for TE and TM modes, respectively.

The two curves show a similar behavior but the n values of our AlN sample are lower than these of the crystal.¹⁵

However, it is not always easy to compare to previous studies on Al_xGa_{1-x}N with x (≤ 0.7) composition such as Hui *et al.*⁹ Nevertheless, compared to Ref. 9 polynomial expression linking the averaged refractive index dependence on the Al molar fraction at 1550 nm, our refractive index values are slightly higher (2.034/2.075 compared to 2.031). This difference could be related to the growth structure²³ but mainly to the different characterization technique used, i.e., optical transmission compared to our Metricon system which is working in reflection mode with polarized incident light.

Several Transmission Electron Microscopy (TEM) studies of our AlN sample have shown a columnar-structured material with a low angle grain boundary separating individual grains. We suggest that the low angle grains which are planar defects can be decomposed into arrays of dislocations and may be responsible for reducing n. This columnar structure could induce volume scattering optical losses.

The birefringence, defined as the difference between the ordinary and the extraordinary refractive indices

TABLE I. Results of the fitting parameters obtained from Fig. 3. The different levels of traps E_{T1} , E_{T2} , E_{T3} , E_{T4} and the parameters A and C are used to determine the capture cross sections (s).

Capture cross-section	E_T (eV)	A	C (eV)	s (cm ²)
$s_B = A (h\nu - E_{T1})^{1/2} / (h\nu(h\nu + E_{T1} + C)^2)$	3.75	1.4×10^{-6}	2400	5×10^{-19}
$s_B = A (h\nu - E_{T2})^{1/2} / (h\nu(h\nu + E_{T2} + C)^2)$	4.4	2.76×10^{-8}	160	1.1×10^{-18}
$s_B = A (h\nu - E_{T3})^{1/2} / (h\nu(h\nu + E_{T3} + C)^2)$	4.79	7.88×10^{-6}	2700	3.49×10^{-18}
$s_C = A (h\nu - E_{T4})^{3/2} / (h\nu)$	5.5	2.1×10^{-11}	...	7.66×10^{-18}

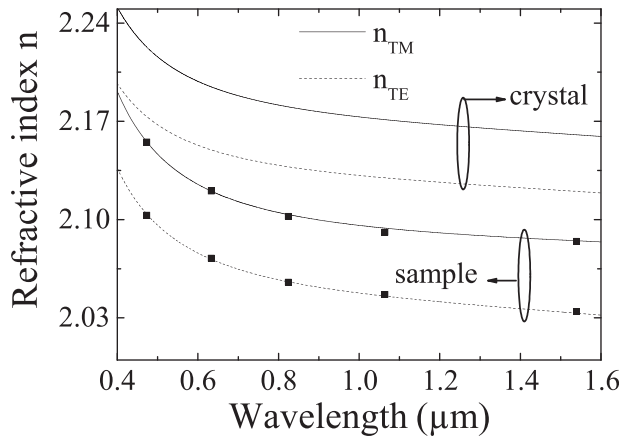


FIG. 4. Dispersion curve of the refractive index in both polarization and comparison with the single crystal values.¹⁵

$\Delta n = n_{TM} - n_{TE}$, is slightly decreasing with the wavelength as the penetration depth of the Gaussian light wave is directly related to the wavelength. In the TM polarization, light electric field is perpendicular to the interface planes, so that n in this polarization is more sensitive to structural defects, such as the dislocations density, which is estimated to be around $5 \times 10^9 \text{ cm}^{-2}$ from TEM analysis.

C. M-lines spectroscopy: Thermo-optics

Temperature dependence of the refractive index is carried out from ambient to 150 °C. A flexible heating plate coupled to a thermo-sensor pad is mounted during the optical measurement, as shown in Fig. 5. For each wavelength, the complete spectrum (all the effective index) is measured to calculate n in each polarization.

Fig. 6 presents the evolution of n with the temperature in both polarizations. Over the whole spectral range, the evolution seems to be linear and an affine law can fit the curves. In the TE polarization, the extracted thermo-optic coefficient $\Delta n/\Delta T$ is quite constant with the wavelength (around 4 to $5 \times 10^{-5} \text{ K}^{-1}$). In the TM polarization, it decreases with the wavelength from 7 to $1 \times 10^{-5} \text{ K}^{-1}$ in the 450–1553 nm spectral range. This evolution behavior was already observed for other materials.⁸

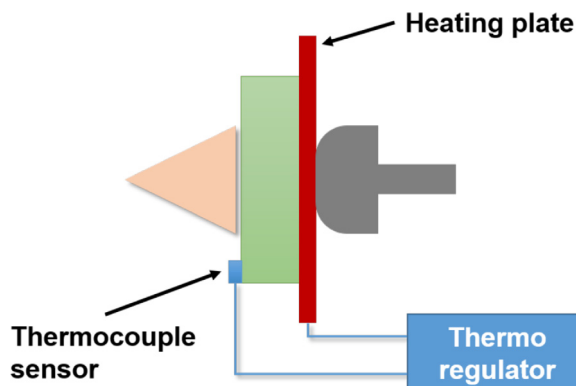


FIG. 5. Schematics of the heating setup added to the Metricon system. The heating plate is pressed against the substrate and a thermo-sensor is placed in the active layer to check the temperature within the AlN layer.

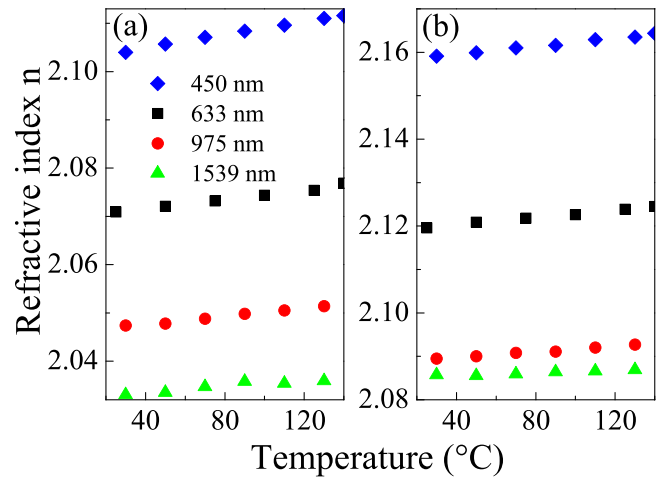


FIG. 6. Temperature dependence of n in (a) TE polarization and (b) in TM polarization at 450, 633, 975, and 1553 nm.

D. M-lines spectroscopy: Propagation loss

The attenuation of the propagating waves is a key parameter for the waveguide design. Surface scattering and absorption are the main loss mechanisms in semiconductor materials.

Tang *et al.*²⁵ reported on low propagation losses for AlN on Al_2O_3 in the visible range and several research groups^{13,29} on other substrates in the infrared range. Fig. 7 presents the measured total propagation losses of our AlN film between 633 nm and 1553 nm wavelength. The laser beam is coupled into the waveguide when exciting the fundamental TE_0 propagation mode. An optical fiber with a core diameter of 1 mm is used as a probe to collect the light scattered in and out from the surface of the waveguide. For UV wavelengths, close to the band-gap value, the light is strongly absorbed on the first centimeter of propagation so that the losses cannot be measured with our Metricon M2010 system. The value per unit of propagation length decreases exponentially with the wavelength with a decay rate of 3.2. When the value in the visible range is compatible with a photodetector application, the best measured value for optical propagation is about 0.7 dB/cm at 1553 nm, taking the total

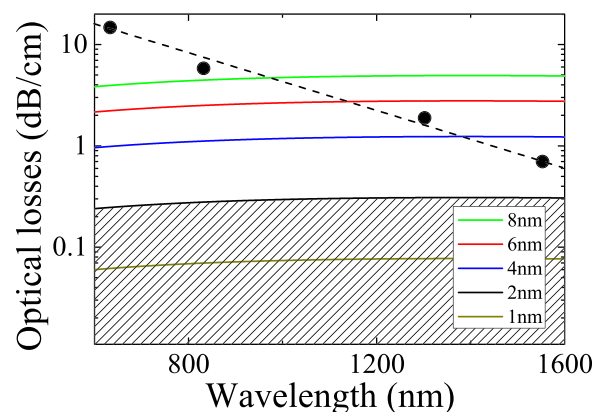


FIG. 7. Evolution of propagation losses at different wavelengths (dots) and calculated scattering optical losses as a function of the wavelength for $m=0$ and for different values of rms roughness (curves) for TE polarization.

TABLE II. Summary of refractive index and propagation losses values at different incident wavelengths. n_{TE} and n_{TM} are the refractive index in the TE and TM polarization, respectively (MND: measurement not done, PM: performed measurement but no result).

λ (μm)	0.453	0.532	0.633	0.824	0.975	1.064	1.302	1.553
α (dB/cm)	PM	PM	14.73	5.82	MND	MND	1.89	0.7
n_{TE}	2.102	2.084	2.071	2.053	2.045	2.045	MND	2.034
n_{TM}	2.157	2.135	2.120	2.101	2.092	2.091	MND	2.075
Δn (10^{-2})	5.49	5.12	4.90	4.84	4.68	4.60	MND	4.14

losses into account. All measured and extracted values are summarized in Table II.

A physical model has been developed to evaluate the contribution of the surface scattering losses; its influence is computed on the total propagation losses (see in Eq. (4)). Surface scattering losses (α_{surf}) are related to the rms deviation of the planarity at the guiding layer interfaces (σ_{xy}). From the atomic force microscopy (AFM) analysis, the surface topography of our sample shows a 2 nm roughness in a $10 \times 10 \mu\text{m}^2$ area (Figure 8) with small crystal nucleation, which is supposed to be the main origin of scattering.

Light intensity decrease through surface scattering at the two interfaces of the guiding layer is given by the model developed by Tien²⁶ through the following attenuation relationship:

$$\alpha_{surf} = \left(\frac{4\pi}{\lambda}\right)^2 \left(\frac{\cos^3 \theta}{2 \sin \theta}\right) \left(\frac{\sigma_{12}^2 + \sigma_{01}^2}{t + 1/p_{10} + 1/p_{12}}\right), \quad (4)$$

where t is the thickness of the guiding layer, $1/p_{10}$ and $1/p_{12}$ are light penetration depths at the guiding/air and the guiding/cladding layer interfaces, respectively. θ is the angle between the light path and the normal of the interfaces in the cladding, guiding layers, and air, λ is the working wavelength, and σ_{01} and σ_{12} represent the roughness at the air/guiding and at the guiding/cladding layer interfaces, respectively. In this model, it is assumed that the roughness σ_{01} and σ_{12} have the same value, called σ .

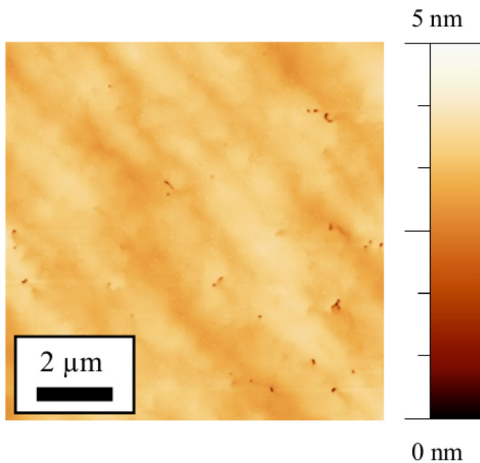


FIG. 8. AFM 2D mapping of the AlN surface sample. The average calculated rms roughness value is 2 nm.

Fig. 7 represents the surface scattering losses evolution calculated as a function of the wavelength for different surface roughness (σ) for TE₀ mode in the case of a planar waveguide. As expected, the surface scattering losses increase strongly with the value of σ . Moreover, for a fixed value of σ , a maximum of scattering losses is obtained for a wavelength in the infrared range (near 1300 nm). By comparing the measured loss values and the theoretical surface scattering contribution, a significant contribution of surface scattering is concluded, especially at 1553 nm wavelength. In the other cases, for the shorter wavelengths, the absorption coefficient of the material or volume scattering are the principal factors of high losses and could explain the evolution of the optical losses as a function of the wavelength. Refractive index and material absorption coefficient increase for shorter wavelengths according to Kramers-Kronig law. In our case, due to the presence of a columnar structure, the derived standard Mie model⁵ reveals that the volume optical losses strongly increase toward the shorter wavelengths. This is a confirmation that the optical propagation properties are here close to single-crystal value of about $0.4 \text{ dB}\cdot\text{cm}^{-1}$ at 1553 nm telecoms wavelength, without taking the surface scattering losses into account. This value is acceptable for optical waveguide applications.¹⁷

IV. CONCLUSION

Our investigation demonstrates that AlN on Al₂O₃ substrate is a versatile structure. With a strong optical absorption in the UV range, it is one of the best candidates for UV photo-detection applications. In the opposite, the best optical propagation loss result of 0.7 dB/cm is obtained at 1553 nm and is mainly due to the surface scattering. That opens the way to develop easy-to-fabricate AlN on Al₂O₃ platform for low-loss optical waveguide applications with a relative good stability with temperature.

ACKNOWLEDGMENTS

The authors are grateful to John Jackson from Metricon Corp., for the technical support provided. This work was funded by the ANR BLAN07-1188059 “HIPPOPP” project. V. Mortet is a J. E. Purkyne (ASCR) research fellowship.

¹H. A. Barkad, A. Soltani, M. Mattalah, J.-C. Gerbedoen, M. Rousseau, J.-C. De Jaeger, A. BenMoussa, V. Mortet, K. Haenen, B. Benbakhti, M. Moreau, R. Dupuis, and A. Ougazzaden, *J. Phys. D: Appl. Phys.* **43**, 465104 (2010).

²A. BenMoussa, J. F. Hochedez, R. Dahal, J. Li, J. Y. Lin, H. X. Jiang, A. Soltani, J.-C. De Jaeger, U. Kroth, and M. Richter, *Appl. Phys. Lett.* **92**, 022108, (2008).

³A. BenMoussa, A. Soltani, J.-C. Gerbedoen, T. Saito, S. Averin, S. Gissot, B. Giordanengo, G. Berger, U. Kroth, J.-C. De Jaeger, and A. Gottwald, *Nucl. Instrum. Methods Phys. Res. B* **312**, 48–53 (2013).

⁴R. H. Bube, *Photoconductivity of Solids* (Wiley, New York, 1960).

⁵A. J. Cox, A. J. DeWeerd, and J. Linden, *Am. J. Phys.* **70**(6), 620–625 (2002).

⁶R. Dahal, T. M. Al Tahtamouni, Z. Y. Fan, J. Y. Lin, and H. X. Jiang, *Appl. Phys. Lett.* **90**, 263505 (2007).

⁷V. Yu. Davydov, Yu. E. Kitaev, I. N. Goncharuk, A. N. Smirnov, J. Graul, O. Semchinova, D. Uffmann, M. B. Smirnov, A. P. Mirgorodsky, and R. A. Evarestov, *Phys. Rev. B* **58**, 12899–12907 (1998).

- ⁸G. Ghosh, *Appl. Opt.* **36**, 1540–1546 (1997).
- ⁹R. Hui, Y. Wan, J. Li, S. Jin, J. Lin, and H. Jing, *IEEE J. Quantum Electron.* **41**, 100 (2005).
- ¹⁰J. C. Inkson, *J. Phys. C: Solid State Phys.* **14**, 1093–1101 (1981).
- ¹¹J. Li, Z. Y. Fan, R. Dahal, M. L. Nakarmi, J. Y. Lin, and H. X. Jiang, *Appl. Phys. Lett.* **89**, 213510 (2006).
- ¹²T. Mattila and R. M. Nieminen, *Phys. Rev. B* **55**, 9571 (1997).
- ¹³T. Matsushima, J. Kawanabe, S. Saimi, and Y. Cho, in 27th International Conference on Infrared and Millimeter Waves (2002), pp. 313–314.
- ¹⁴I. Gorczyca, N. E. Christensen, and A. Svane, *Phys. Rev. B* **66**, 075210 (2002).
- ¹⁵M. Bass, C. DeCusatis, J. Enoch, V. Lakshminarayanan, G. Li, C. MacDonald, V. Mahajan, and E. Van Stryland, “HandBook of Optics (3rd Edition of Vol. II): Design, Fabrication and Testing, Sources and Detectors, Radiometry and Photometry,” 2009. Available at <http://www.mhprofessional.com/product.php?isbn=0071498907>.
- ¹⁶W. H. P. Pernice, C. Xiong, and H. X. Tang, *Opt. Express* **20**, 12261–12269 (2012).
- ¹⁷W. H. P. Pernice, C. Xiong, C. Schuck, and H. X. Tang, *Appl. Phys. Lett.* **100**, 223501 (2012).
- ¹⁸M. Razeghi, *Proc. IEEE* **90**(6), 1006–1014 (2002).
- ¹⁹C. Stampfl and C. G. Van de Walle, *Appl. Phys. Lett.* **72**, 459 (1998).
- ²⁰C. Stampfl and C. G. Van de Walle, *Phys. Rev. B* **65**, 155212 (2002).
- ²¹L. Silvestri, K. Dunn, S. Praver, and F. Ladouceur, *EPL* **98**, 36003 (2012).
- ²²A. Stolz, E. Cho, Y. Androussi, D. Troadec, E. Dogheche, D. Pavlidis, and D. Decoster, *Appl. Phys. Lett.* **98**, 161903 (2011).
- ²³A. Stolz, A. Soltani, A. Abdallah, J. Charrier, D. Deresmes, P.-Y. Jouan, and J.-C. De Jaeger, *Thin Solid Films* **534**, 442 (2013).
- ²⁴A. Talbi, A. Soltani, V. Mortet, J.-C. Gerbedoen, J.-C. De Jaeger, and P. Pernod, *Diamond Relat. Mater.* **22**, 66–69 (2012).
- ²⁵X. Tang, Y. Yuan, K. Wongchotigul, and M. G. Spencer, *Appl. Phys. Lett.* **70**, 3206 (1997).
- ²⁶P. K. Tien, *Appl. Opt.* **10**, 2395–2413 (1971).
- ²⁷R. Ulrich and R. Torge, *Appl. Opt.* **12**(12), 2901–2908 (1973).
- ²⁸F. Urbach, *Phys. Rev.* **92**, 1324 (1953).
- ²⁹C. Xiong, W. H. P. Pernice, and H. X. Tang, *Nano Lett.* **12**, 3562–3568 (2012).